

Application of the MLPG to Thermo-Piezoelectricity

J. Sladek¹, V. Sladek¹, Ch. Zhang² and P. Sölek³

Abstract: A meshless method based on the local Petrov-Galerkin approach is proposed for the solution of boundary value problems for coupled thermo-electro-mechanical fields. Transient dynamic governing equations are considered here. To eliminate the time-dependence in these equations, the Laplace-transform technique is applied. Material properties of piezoelectric materials are influenced by a thermal field. It is leading to an induced nonhomogeneity and the governing equations are more complicated than in a homogeneous counterpart. Two-dimensional analyzed domain is subdivided into small circular subdomains surrounding nodes randomly spread over the whole domain. A unit step function is used as the test functions in the local weak-form. The derived local integral equations (LIEs) have boundary-domain integral form. The moving least-squares (MLS) method is adopted for the approximation of the physical quantities in the LIEs. The Stehfest's inversion method is applied to obtain the final time-dependent solutions.

Keyword: Meshless local Petrov-Galerkin method (MLPG), Moving least-squares interpolation, piezoelectric solids, orthotropic properties, transient thermal load, Laplace-transform

1 Introduction

Piezoelectric materials have wide range engineering applications in smart structures and devices. They are extensively utilized as transducers, sensors and actuators in many engineering fields. Piezoelectric materials have usually anisotropic

properties. Except this complication electric and mechanical fields are coupled each other and the governing equations are much more complex than those in the classical elasticity. Thus, efficient computational methods to solve the boundary or the initial-boundary value problems for piezoelectric solids are required. Mostly, the finite element method (FEM) [Gruebner et al. (2003); Govorukha and Kamlah (2004); Enderlein et al. (2005), Kuna (2006)] and the boundary element method (BEM) [Pan (1999); Lee (1995); Ding and Liang (1999); Gross et al. (2005); Garcia-Sanchez et al. (2005, 2007); Saez et al. (2006); Sheng and Sze (2006)] are applied to solve general piezoelectric problems. Recently, also meshless methods have been successfully applied to piezoelectric problems [Ohs and Aluru (2001); Liu et al. (2002)].

Certain piezoelectric materials are also temperature sensitive, i.e. an electric charge or voltage is generated when temperature variations are exposed. This effect is called the pyroelectric effect. If a temperature load is considered in a piezoelectric solid it is needed to take into account a coupling of thermo-electro-mechanical fields. The theory of thermo-piezoelectricity was for the first time proposed by Mindlin (1961). The physical laws for thermo-piezoelectric materials have been explored by Nowacki (1978). Dunn (1993) studied micromechanics models for effective thermal expansion and pyroelectric coefficients of piezoelectric composites. Ashida et al. (1994) introduced a technique for three-dimensional axisymmetric problems of piezothermoelasticity. Shang et al. (1996) proposed a method for three-dimensional axisymmetric problems of transversally isotropic thermo-piezoelectric materials by means of potential functions and Fourier-Hankel transformations. Fracture and damage behaviours of a cracked piezoelectric solid under coupled

¹Institute of Construction and Architecture, Slovak Academy of Sciences, 84503 Bratislava, Slovakia

²Department of Civil Engineering, University of Siegen, D-57068 Siegen, Germany

³Department of Mechanics, Slovak Technical University, Bratislava, Slovakia

thermal, mechanical and electrical loads have been studied by Yu and Qin (1996a,b). A review on fracture of thermo-piezoelectric materials is given by Qin (2001). Boundary value problems for coupled fields are complex. Analytical methods can be only applied to simple problems of thermo-piezoelectricity [Tsamasphyros and Song (2005); Shang et al. (2003a,b)]. However, the analysis and the design process of smart engineering structures with integrated piezoelectric actuators or sensors require powerful calculation tools. Up to now the finite element methods (FEM) provides an effective technique [Tzou and Ye (1994); Gornandt and Gabbert (2002); Shang et al. (2002); Kuna (2006)] in a homogeneous medium. Rao and Sunar (1993) investigated the piezothermoelectric problem of intelligent structures with distributed piezoelectric sensors and actuators and concluded that the inclusion of the thermal effects may help improve the performance characteristics of the system.

Most investigations in piezothermoelasticity were done under the assumption of the temperature independent material properties. However, material properties under a thermal load are influenced by temperature. Bert and Birman (1999) showed that the piezoelectric coefficients are stress and electric-field dependent. If this phenomenon is considered the material properties are continuously varying with Cartesian coordinates. In this so called induced nonhomogeneity the governing equations are more complicated than in a homogeneous counterpart. Some relative simple problems of coupled electro-mechanical fields in continuously nonhomogeneous solids have been successfully solved in previous works [Zhu et al. (1995, 1999); Li and Weng (2002); Ueda (2003)]. Recently, Han et al. (2006) analyzed responses of piezoelectric, transversally isotropic, functionally graded and multilayered half spaces to uniform circular surface loading. As far as the authors are aware, very limited works can be found in the literature for the active control of functionally graded material (FGM) structures using piezoelectric materials. Liew et al. (2001) presented the finite element formulation based on the first-order shear deformation theory for static and

dynamic piezothermoelastic analysis and active control of FGM plates subjected to a thermal load. The first attempt to solve induced nonhomogeneity problem in thermo-piezoelectricity for an infinite and half-space was given by Aouadi (2006). A general numerical solution for induced nonhomogeneity problem in thermo-piezoelectricity is not available according to the best of the author's knowledge.

The meshless local Petrov-Galerkin (MLPG) method is a fundamental base for the derivation of many meshless formulations, since trial and test functions can be chosen from different functional spaces. The MLPG method with a Heaviside step function as the test functions [Atluri et al. (2003); Atluri (2004); Sladek et al. (2004)] has been applied to solve 2-D homogeneous piezoelectric problems [Sladek et al. (2006)]. Usually meshless approximations involve more nodes than in a conventional polynomial approximation and the required shape functions are more complex. To reduce the computing time in the MLPG, a mixed formulation [Atluri et al. (2006)] can be applied, which reduces the radius of the support domain at the same accuracy as in the traditional approximation. Since a smaller size of the support domain decreases the bandwidth of the system matrix, the computing time can be significantly reduced.

Recently, authors have applied a meshless method (MLPG) to analyze continuously nonhomogeneous piezoelectric solids under a mechanical or electrical load [Sladek et al. (2007)]. In the present paper, the MLPG method is extended to 2-D thermo-piezoelectric solids with induced nonhomogeneity. The coupled thermo-electromechanical fields in thermo-piezoelectricity are described by partial differential equations, where mechanical fields are described by the equations of motion with an inertial term. Maxwell's equation for the electrical field has a quasi-static character and thermal field is described by the heat conduction equation, which has a diffusive character. To eliminate the time-dependences in the governing partial differential equations, the Laplace-transform technique is applied such that they are satisfied in the Laplace-transformed domain in a weak-form on small fic-

titious subdomains. Since all three fields are mutually coupled in constitutive equations, also the Maxwell's equation has to be written in the Laplace-transform domain. Nodal points are introduced and spread on the analyzed domain and each node is surrounded by a small circle for simplicity, but without loss of generality. For a simple shape of subdomains like circles applied in this paper, numerical integrations over them can be easily carried out. The integral equations have a very simple nonsingular form. The spatial variations of the displacements, the electric potential and the temperature are approximated by the Moving Least-Squares (MLS) scheme [Belytschko et al. (1996); Zhu et al. (1998)]. After performing the spatial integrations, a system of linear algebraic equations for the unknown nodal values is obtained. The boundary conditions on the global boundary are satisfied by the collocation of the MLS-approximation expressions for the displacements, the electric potential and the temperature at the boundary nodal points. The Stehfest's inversion method [Stehfest (1970)] is applied to obtain the final time-dependent solutions. The accuracy and the efficiency of the proposed MLPG method are verified by several numerical examples.

2 Governing equations for thermo-electro-mechanical fields

Under the quasi-electrostatic assumption the governing equations for thermo-piezoelectricity in continuously nonhomogeneous solids are given by the equation of motion for displacements, the first Maxwell's equation for the vector of electric displacements and heat conduction equation [Mindlin (1974)]

$$\sigma_{ij,j}(\mathbf{x}, \tau) + X_i(\mathbf{x}, \tau) = \rho(\mathbf{x})\ddot{u}_i(\mathbf{x}, \tau), \quad (1)$$

$$D_{j,j}(\mathbf{x}, \tau) - R(\mathbf{x}, \tau) = 0, \quad (2)$$

$$[k_{ij}(\mathbf{x})\theta_{,j}(\mathbf{x}, \tau)]_{,i} - \rho(\mathbf{x})c(\mathbf{x})\dot{\theta}(\mathbf{x}, \tau) + S(\mathbf{x}, \tau) = 0, \quad (3)$$

where σ_{ij} , τ , θ , u_i , D_i , X_i , R and S are the stress, time, temperature difference, displacement, electric displacement, density of body force vector, volume density of free charges and density of

heat sources, respectively. Also, ρ , k_{ij} and c are the mass density, thermal conductivity tensor and specific heat, respectively. The dots over a quantity indicate the time derivatives. A static problem can be considered formally as a special case of the dynamic one, by omitting the acceleration $\ddot{u}_i(\mathbf{x}, \tau)$ in the equations of motion (1) and the time derivative terms in equation (3). Therefore, both cases are analyzed in this paper.

For most materials the inverse thermoelastic and pyroelectric effects are very weak, i.e. the heat generation by mechanical and electrical fields can be neglected. Then, the constitutive relations representing the partially-coupling of the mechanical, electrical and thermal fields are given by

$$\sigma_{ij}(\mathbf{x}, \tau) = c_{ijkl}(\mathbf{x})\varepsilon_{kl}(\mathbf{x}, \tau) - e_{kij}(\mathbf{x})E_k(\mathbf{x}, \tau) - \gamma_{ij}(\mathbf{x})\theta(\mathbf{x}, \tau), \quad (4)$$

$$D_j(\mathbf{x}, \tau) = e_{jkl}(\mathbf{x})\varepsilon_{kl}(\mathbf{x}, \tau) + h_{jk}(\mathbf{x})E_k(\mathbf{x}, \tau) + p_j(\mathbf{x})\theta(\mathbf{x}, \tau), \quad (5)$$

where $c_{ijkl}(\mathbf{x})$, $e_{jkl}(\mathbf{x})$, $h_{jk}(\mathbf{x})$ and $p_j(\mathbf{x})$ are the elastic, piezoelectric, dielectric and pyroelectric material tensors in a continuously nonhomogeneous piezoelectric medium, respectively. The stress-temperature modulus $\gamma_{ij}(\mathbf{x})$ can be expressed through the stiffness coefficients and the coefficients of linear thermal expansion α_{kl}

$$\gamma_{ij} = c_{ijkl}\alpha_{kl}. \quad (6)$$

The strain tensor ε_{ij} and the electric field vector E_j are related to the displacements u_i and the electric potential ψ by

$$\varepsilon_{ij} = \frac{1}{2}(u_{i,j} + u_{j,i}), \quad (7)$$

$$E_j = -\psi_{,j}. \quad (8)$$

For plane problems the constitutive equations are frequently written in terms of the second-order tensor of elastic constants [Lekhnitskii (1963)]. Many piezoelectric solids are transversely isotropic. Under the plane strain condition with $\varepsilon_{33} = \varepsilon_{31} = \varepsilon_{32} = E_3 = 0$, the constitu-

to [Sheng and Size (2006)]

$$\begin{aligned} \begin{bmatrix} \sigma_{11} \\ \sigma_{22} \\ \sigma_{12} \end{bmatrix} &= \begin{bmatrix} c_{11} & c_{12} & 0 \\ c_{12} & c_{22} & 0 \\ 0 & 0 & c_{66} \end{bmatrix} \begin{bmatrix} \varepsilon_{11} \\ \varepsilon_{22} \\ 2\varepsilon_{12} \end{bmatrix} \\ &\quad - \begin{bmatrix} 0 & e_{21} \\ 0 & e_{22} \\ e_{15} & 0 \end{bmatrix} \begin{bmatrix} E_1 \\ E_2 \end{bmatrix} - \boldsymbol{\gamma}\theta \\ &= \mathbf{C}(\mathbf{x}) \begin{bmatrix} \varepsilon_{11} \\ \varepsilon_{22} \\ 2\varepsilon_{12} \end{bmatrix} - \mathbf{L}(\mathbf{x}) \begin{bmatrix} E_1 \\ E_2 \end{bmatrix} - \boldsymbol{\gamma}\theta, \end{aligned} \quad (9)$$

$$\begin{aligned} \begin{bmatrix} D_1 \\ D_2 \end{bmatrix} &= \begin{bmatrix} 0 & 0 & e_{15} \\ e_{21} & e_{22} & 0 \end{bmatrix} \begin{bmatrix} \varepsilon_{11} \\ \varepsilon_{22} \\ 2\varepsilon_{12} \end{bmatrix} \\ &\quad + \begin{bmatrix} h_{11} & 0 \\ 0 & h_{22} \end{bmatrix} \begin{bmatrix} E_1 \\ E_2 \end{bmatrix} + \begin{bmatrix} p_1 \\ p_2 \end{bmatrix} \theta \\ &= \mathbf{G}(\mathbf{x}) \begin{bmatrix} \varepsilon_{11} \\ \varepsilon_{22} \\ 2\varepsilon_{12} \end{bmatrix} + \mathbf{H}(\mathbf{x}) \begin{bmatrix} E_1 \\ E_2 \end{bmatrix} + \mathbf{P}(\mathbf{x})\theta, \end{aligned} \quad (10)$$

where

$$\boldsymbol{\gamma} = \begin{bmatrix} c_{11} & c_{12} & c_{13} \\ c_{12} & c_{22} & c_{23} \\ 0 & 0 & 0 \end{bmatrix} \begin{bmatrix} \alpha_{11} \\ \alpha_{22} \\ \alpha_{33} \end{bmatrix} = \begin{bmatrix} \gamma_{11} \\ \gamma_{22} \\ 0 \end{bmatrix}.$$

The following essential and natural boundary conditions are assumed for the mechanical field

$$\begin{aligned} u_i(\mathbf{x}, \tau) &= \tilde{u}_i(\mathbf{x}, \tau), & \text{on } \Gamma_u, \\ t_i(\mathbf{x}, \tau) &= \sigma_{ij}n_j = \tilde{t}_i(\mathbf{x}, \tau), & \text{on } \Gamma_t, \end{aligned}$$

for the electrical field

$$\begin{aligned} \psi(\mathbf{x}) &= \tilde{\psi}(\mathbf{x}), & \text{on } \Gamma_p, \\ n_i D_i(\mathbf{x}) &= \tilde{Q}(\mathbf{x}), & \text{on } \Gamma_q, \end{aligned}$$

and for the thermal field

$$\begin{aligned} \theta(\mathbf{x}, \tau) &= \tilde{\theta}(\mathbf{x}, \tau), & \text{on } \Gamma_a, \\ q(\mathbf{x}, \tau) &= k_{ij}\theta_{,j}(\mathbf{x}, \tau)n_i(\mathbf{x}) = \tilde{q}(\mathbf{x}, \tau), & \text{on } \Gamma_b, \end{aligned}$$

where Γ_u is the part of the global boundary with prescribed displacements, and on Γ_t , Γ_p , Γ_q , Γ_a , and Γ_b the traction vector, the electric potential,

the surface charge density, the temperature and the heat flux are prescribed, respectively.

Initial conditions for the mechanical and thermal quantities are assumed as

$$\begin{aligned} u_i(\mathbf{x}, \tau)|_{\tau=0} &= u_i(\mathbf{x}, 0) \text{ and } \dot{u}_i(\mathbf{x}, \tau)|_{\tau=0} = \dot{u}_i(\mathbf{x}, 0) \\ \theta(\mathbf{x}, \tau)|_{\tau=0} &= \theta(\mathbf{x}, 0) \text{ in } \Omega. \end{aligned}$$

Applying the Laplace-transform to the governing equations (1) and (3) we obtain

$$\bar{\sigma}_{ij,j}(\mathbf{x}, p) - \rho(\mathbf{x})p^2\bar{u}_i(\mathbf{x}, p) = -\bar{F}_i(\mathbf{x}, p), \quad (11)$$

$$\begin{aligned} [k_{ij}(\mathbf{x})\bar{\theta}_{,j}(\mathbf{x}, p)]_{,i} - \rho(\mathbf{x})c(\mathbf{x})p\bar{\theta}(\mathbf{x}, p) \\ + \bar{W}(\mathbf{x}, p) = 0, \end{aligned} \quad (12)$$

where

$$\begin{aligned} \bar{F}_i(\mathbf{x}, p) &= \bar{X}_i(\mathbf{x}, p) + pu_i(\mathbf{x}, 0) + \dot{u}_i(\mathbf{x}, 0), \\ \bar{W}(\mathbf{x}, p) &= \bar{S}(\mathbf{x}, p) + \theta(\mathbf{x}, 0) \end{aligned}$$

are the re-defined body forces and heat source, respectively, in the Laplace-transformed domain with the initial boundary conditions for the displacements $u_i(\mathbf{x}, 0)$, velocities $\dot{u}_i(\mathbf{x}, 0)$ and temperature $\theta(\mathbf{x}, 0)$.

The Laplace-transform of a function $f(\mathbf{x}, \tau)$ is defined as

$$L[f(x, \tau)] = \bar{f}(x, p) = \int_0^{\infty} f(x, \tau)e^{-p\tau}d\tau,$$

where p is the Laplace-transform parameter.

3 Local integral equation formulation

Instead of writing the global weak-form for the above governing equations, we apply the MLPG method to construct a weak-form over the local fictitious subdomains such as Ω_s , which is a small region taken for each node inside the global domain [Atluri and Zhu (1998); Atluri (2004)]. The local subdomains overlap each other, and cover the whole global domain Ω . The local subdomains could be of any geometrical shape and size. In the present paper, the local subdomains are

taken to be of the circular shape. The local weak-form of the governing equations (11) can be written as

$$\int_{\Omega_s} [\bar{\sigma}_{ij,j}(\mathbf{x}, p) - \rho(\mathbf{x})p^2\bar{u}_i(\mathbf{x}, p) + \bar{F}_i(\mathbf{x}, p)] u_{ik}^*(\mathbf{x}) d\Omega = 0, \quad (13)$$

where $u_{ik}^*(\mathbf{x})$ is a test function.

Using

$$\bar{\sigma}_{ij,j} u_{ik}^* = (\bar{\sigma}_{ij} u_{ik}^*)_{,j} - \bar{\sigma}_{ij} u_{ik,j}^*$$

and applying the Gauss divergence theorem one can write

$$\begin{aligned} & \int_{\partial\Omega_s} \bar{\sigma}_{ij}(\mathbf{x}, p) n_j(\mathbf{x}) u_{ik}^*(\mathbf{x}) d\Gamma \\ & - \int_{\Omega_s} \bar{\sigma}_{ij}(\mathbf{x}, p) u_{ik,j}^*(\mathbf{x}) d\Omega \\ & + \int_{\Omega_s} [\bar{F}_i(\mathbf{x}, p) - \rho(\mathbf{x})p^2\bar{u}_i(\mathbf{x}, p)] u_{ik}^*(\mathbf{x}) d\Omega \\ & = 0, \end{aligned} \quad (14)$$

where $\partial\Omega_s$ is the boundary of the local subdomain which consists of three parts $\partial\Omega_s = L_s \cup \Gamma_{st} \cup \Gamma_{su}$ [Atluri (2004)]. Here L_s is the local boundary that is totally inside the global domain, Γ_{st} is the part of the local boundary which coincides with the global traction boundary, i.e., $\Gamma_{st} = \partial\Omega_s \cap \Gamma_t$, and similarly Γ_{su} is the part of the local boundary that coincides with the global displacement boundary, i.e., $\Gamma_{su} = \partial\Omega_s \cap \Gamma_u$.

By choosing a Heaviside step function as the test function $u_{ik}^*(\mathbf{x})$ in each subdomain

$$u_{ik}^*(\mathbf{x}) = \begin{cases} \delta_{ik} & \text{at } \mathbf{x} \in \Omega_s \\ 0 & \text{at } \mathbf{x} \notin \Omega_s \end{cases}$$

the local weak-form (14) is then converted into the following local boundary-domain integral equations

$$\begin{aligned} & \int_{L_s + \Gamma_{su}} \bar{t}_i(\mathbf{x}, p) d\Gamma - \int_{\Omega_s} \rho(\mathbf{x})p^2\bar{u}_i(\mathbf{x}, p) d\Omega \\ & = - \int_{\Gamma_{st}} \bar{t}_i(\mathbf{x}, p) d\Gamma - \int_{\Omega_s} \bar{F}_i(\mathbf{x}, p) d\Omega. \end{aligned} \quad (15)$$

Note that the local integral equations (15) are valid for both homogeneous and nonhomogeneous linear piezoelectric solids. Nonhomogeneous material properties are included in eq. (15) through the elastic and piezoelectric tensor of the material coefficients in the traction components.

Similarly, the local weak form of the governing equation (2) rewritten for the Laplace-transforms is given by

$$\int_{\Omega_s} [\bar{D}_{j,j}(\mathbf{x}, p) - \bar{R}(\mathbf{x}, p)] v^*(\mathbf{x}) d\Omega = 0, \quad (16)$$

where $v^*(\mathbf{x})$ is a test function.

Applying the Gauss divergence theorem to the local weak-form and considering the Heaviside step function for the test function $v^*(\mathbf{x})$, one obtains

$$\begin{aligned} & \int_{L_s + \Gamma_{sp}} \bar{Q}(\mathbf{x}, p) d\Gamma \\ & = - \int_{\Gamma_{sq}} \bar{Q}(\mathbf{x}, p) d\Gamma + \int_{\Omega_s} \bar{R}(\mathbf{x}, p) d\Omega, \end{aligned} \quad (17)$$

where

$$\begin{aligned} \bar{Q}(\mathbf{x}, p) &= \bar{D}_{j,j}(\mathbf{x}, p) n_j \\ &= [e_{jkl} \bar{u}_{k,l}(\mathbf{x}, p) - h_{jk} \bar{\psi}_{,k}(\mathbf{x}, p)] n_j. \end{aligned}$$

The local weak-form of the diffusion equation (12) can be written as

$$\int_{\Omega_s} \left\{ [k_{ij}(\mathbf{x}) \bar{\theta}_{,j}(\mathbf{x}, p)]_{,i} \mathbf{x} \cdot \mathbf{n} \right. \quad v$$

spaces. For internal nodes, the test function is chosen as the Heaviside step function with its support on the local subdomain. The trial functions, on the other hand, are chosen to be the moving least-squares (MLS) approximation over a number of nodes spread within the domain of influence. The approximated functions for the Laplace-transforms of the mechanical displacements, the electric potential and the temperature can be written as [Atluri (2004)]

$$\begin{aligned}\bar{\mathbf{u}}^h(\mathbf{x}, p) &= \mathbf{\Phi}^T(\mathbf{x}) \cdot \hat{\mathbf{u}}(p) = \sum_{a=1}^n \phi^a(\mathbf{x}) \hat{\mathbf{u}}^a(p), \\ \bar{\psi}^h(\mathbf{x}, p) &= \sum_{a=1}^n \phi^a(\mathbf{x}) \hat{\psi}^a(p), \\ \bar{\theta}^h(\mathbf{x}, p) &= \sum_{a=1}^n \phi^a(\mathbf{x}) \hat{\theta}^a(p),\end{aligned}\quad (20)$$

where the nodal values $\hat{\mathbf{u}}^a(p)$, $\hat{\psi}^a(p)$ and $\hat{\theta}^a(p)$ are fictitious parameters for the displacements, the electric potential and the temperature, respectively, and $\phi^a(\mathbf{x})$ is the shape function associated with the node a . The number of nodes n used for the approximation is determined by the weight function $w^a(\mathbf{x})$. A 4th order spline type weight function is applied in the present work

$$w^a(\mathbf{x}) = \begin{cases} 1 - 6\left(\frac{d^a}{r^a}\right)^2 + 8\left(\frac{d^a}{r^a}\right)^3 - 3\left(\frac{d^a}{r^a}\right)^4, & 0 \leq d^a \leq r^a \\ 0, & d^a \geq r^a \end{cases}, \quad (21)$$

where $d^a = \|\mathbf{x} - \mathbf{x}^a\|$ and r^a is the size of the support domain. It is seen that the C^1 -continuity is ensured over the entire domain, therefore the continuity conditions of the tractions, the electric charge and the heat flux are satisfied.

The Laplace-transform of the traction vector $\bar{\mathbf{t}}_i(\mathbf{x}, p)$ at a boundary point $\mathbf{x} \in \partial\Omega_s$ is approximated in terms of the same nodal values $\hat{\mathbf{u}}^a(p)$ as

$$\begin{aligned}\bar{\mathbf{t}}^h(\mathbf{x}, p) &= \mathbf{N}(\mathbf{x})\mathbf{C}(\mathbf{x}) \sum_{a=1}^n \mathbf{B}^a(\mathbf{x}) \hat{\mathbf{u}}^a(p) \\ &+ \mathbf{N}(\mathbf{x})\mathbf{L}(\mathbf{x}) \sum_{a=1}^n \mathbf{A}^a(\mathbf{x}) \hat{\psi}^a(p) \\ &- \mathbf{N}(\mathbf{x})\boldsymbol{\gamma} \sum_{a=1}^n \phi^a(\mathbf{x}) \hat{\theta}^a(p),\end{aligned}\quad (22)$$

where the matrix $\mathbf{N}(\mathbf{x})$ is related to the normal vector $\mathbf{n}(\mathbf{x})$ on $\partial\Omega_s$ by

$$\mathbf{N}(\mathbf{x}) = \begin{bmatrix} n_1 & 0 & n_2 \\ 0 & n_2 & n_1 \end{bmatrix},$$

and the matrices \mathbf{B}^a and \mathbf{A}^a are represented by the gradients of the shape functions as

$$\mathbf{B}^a(\mathbf{x}) = \begin{bmatrix} \phi_{,1}^a & 0 \\ 0 & \phi_{,2}^a \\ \phi_{,2}^a & \phi_{,1}^a \end{bmatrix}, \quad \mathbf{A}^a(\mathbf{x}) = \begin{bmatrix} \phi_{,1}^a \\ \phi_{,2}^a \end{bmatrix}.$$

Similarly the Laplace-transform of the electrical charge $\bar{Q}(\mathbf{x}, p)$ can be approximated by

$$\begin{aligned}\bar{Q}^h(\mathbf{x}, p) &= \mathbf{N}_1(\mathbf{x})\mathbf{G}(\mathbf{x}) \sum_{a=1}^n \mathbf{B}^a(\mathbf{x}) \hat{\mathbf{u}}^a(p) \\ &- \mathbf{N}_1(\mathbf{x})\mathbf{H}(\mathbf{x}) \sum_{a=1}^n \mathbf{A}^a(\mathbf{x}) \hat{\psi}^a(p) \\ &+ \mathbf{N}_1(\mathbf{x})\mathbf{P}(\mathbf{x}) \sum_{a=1}^n \phi^a(\mathbf{x}) \hat{\theta}^a(p),\end{aligned}\quad (23)$$

where the matrices \mathbf{G} and \mathbf{H} are defined in eq. (10) and

$$\mathbf{N}_1(\mathbf{x}) = \begin{bmatrix} n_1 & n_2 \end{bmatrix}.$$

The Laplace-transform of the heat flux $\bar{q}(\mathbf{x}, p)$ is approximated by

$$\begin{aligned}\bar{q}^h(\mathbf{x}, p) &= k_{ij}n_i \sum_{a=1}^n \phi_{,j}^a(\mathbf{x}) \hat{\theta}^a(p) \\ &= \mathbf{N}_1(\mathbf{x})\mathbf{K}(\mathbf{x}) \sum_{a=1}^n \mathbf{A}^a(\mathbf{x}) \hat{\theta}^a(p),\end{aligned}\quad (24)$$

$$\text{where } \mathbf{K}(\mathbf{x}) = \begin{bmatrix} k_{11} & k_{12} \\ k_{12} & k_{22} \end{bmatrix}.$$

O obeying the boundary conditions at those nodal points on the global boundary, where the displacements, the electrical potential and the temperature are prescribed, and making use of the approximation formula (20), one obtains the discretized form of the boundary conditions as

$$\sum_{a=1}^n \phi^a(\zeta) \hat{\mathbf{u}}^a(p) = \tilde{\mathbf{u}}(\zeta, p) \quad \text{for } \zeta \in \Gamma_u, \quad (25)$$

$$\sum_{a=1}^n \phi^a(\zeta) \hat{\psi}^a(p) = \tilde{\psi}(\zeta, p) \quad \text{for } \zeta \in \Gamma_p, \quad (26)$$

$$\sum_{a=1}^n \phi^a(\zeta) \hat{\theta}^a(p) = \tilde{\theta}(\zeta, p) \quad \text{for } \zeta \in \Gamma_a. \quad (27)$$

Furthermore, in view of the MLS-approximation (22) - (24) for the unknown quantities in the local boundary-domain integral equations (15), (17) and (19), we obtain their discretized forms as

$$\begin{aligned} & \sum_{a=1}^n \left(\int_{L_s + \Gamma_{su}} \mathbf{N}(\mathbf{x}) \mathbf{C}(\mathbf{x}) \mathbf{B}^a(\mathbf{x}) d\Gamma \right. \\ & \quad \left. - \mathbf{I} \rho p^2 \int_{\Omega_s} \phi^a(\mathbf{x}) d\Omega \right) \hat{\mathbf{u}}^a(p) \\ & + \sum_{a=1}^n \left(\int_{L_s + \Gamma_{su}} \mathbf{N}(\mathbf{x}) \mathbf{L}(\mathbf{x}) \mathbf{A}^a(\mathbf{x}) d\Gamma \right) \hat{\psi}^a(p) \\ & - \sum_{a=1}^n \left(\int_{L_s + \Gamma_{su}} \mathbf{N}(\mathbf{x}) \boldsymbol{\gamma}(\mathbf{x}) \phi^a(\mathbf{x}) d\Gamma \right) \hat{\theta}^a(p) \\ & = - \int_{\Gamma_{st}} \tilde{\mathbf{t}}(\mathbf{x}, p) d\Gamma - \int_{\Omega_s} \bar{\mathbf{F}}(\mathbf{x}, p) d\Omega, \quad (28) \end{aligned}$$

$$\begin{aligned} & \sum_{a=1}^n \left(\int_{L_s + \Gamma_{sp}} \mathbf{N}_1(\mathbf{x}) \mathbf{G}(\mathbf{x}) \mathbf{B}^a(\mathbf{x}) d\Gamma \right) \hat{\mathbf{u}}^a(p) \\ & - \sum_{a=1}^n \left(\int_{L_s + \Gamma_{sp}} \mathbf{N}_1(\mathbf{x}) \mathbf{H}(\mathbf{x}) \mathbf{A}^a(\mathbf{x}) d\Gamma \right) \hat{\psi}^a(p) \\ & + \sum_{a=1}^n \left(\int_{L_s + \Gamma_{sp}} \mathbf{N}_1(\mathbf{x}) \mathbf{P}(\mathbf{x}) \phi^a(\mathbf{x}) d\Gamma \right) \hat{\theta}^a(p) \\ & = - \int_{\Gamma_{sq}} \tilde{\mathbf{Q}}(\mathbf{x}, p) d\Gamma + \int_{\Omega_s} \bar{\mathbf{R}}(\mathbf{x}, p) d\Omega, \quad (29) \end{aligned}$$

$$\begin{aligned} & \sum_{a=1}^n \left(\int_{L_s + \Gamma_{sa}} \mathbf{N}_1(\mathbf{x}) \mathbf{K}(\mathbf{x}) \mathbf{A}^a(\mathbf{x}) d\Gamma \right. \\ & \quad \left. - \int_{\Omega_s} \rho c p \phi^a(\mathbf{x}) d\Gamma \right) \hat{\theta}^a(p) \\ & = - \int_{\Gamma_{sb}} \tilde{q}(\mathbf{x}, p) d\Gamma - \int_{\Omega_s} \bar{\mathbf{W}}(\mathbf{x}, p) d\Omega, \quad (30) \end{aligned}$$

which are considered on the sub-domains adjacent to interior nodes as well as to the boundary

nodes on Γ_{st} , Γ_{sq} and Γ_{sb} . In equation (28), \mathbf{I} is a unit matrix defined by

$$\mathbf{I} = \begin{pmatrix} 1 & 0 \\ 0 & 1 \end{pmatrix}.$$

Collecting the discretized local boundary-domain integral equations together with the discretized boundary conditions for the displacements, the electrical potential and the temperature results in the complete system of linear algebraic equations for the computation of the nodal unknowns, namely, the Laplace-transforms of the fictitious parameters $\hat{\mathbf{u}}^a(p)$, $\hat{\psi}^a(p)$ and $\hat{\theta}^a(p)$. The time dependent values of the transformed quantities can be obtained by an inverse Laplace-transform. In the present analysis, the Stehfest's inversion algorithm [Stehfest (1970)] is used.

In previous formulations we have considered a general variation of material properties with Cartesian coordinates. If material parameters are dependent on temperature, one can write for a general material parameter

$$A(\mathbf{x}) = f(\theta(\mathbf{x})). \quad (31)$$

Replacing material parameters by the above expression in constitutive equations (4) and (5), a nonlinear expression is obtained. An iterative approach has to be applied and the linearized constitutive equations in the k-th iteration step can be written as

$$\begin{aligned} \sigma_{ij}^{(k)}(\mathbf{x}, \tau) &= c_{ijkl}^{(k-1)}(\theta) \varepsilon_{kl}^{(k)}(\mathbf{x}, \tau) \\ &\quad - e_{kij}^{(k-1)}(\theta) E_k^{(k)}(\mathbf{x}, \tau) - \gamma_{ij}^{(k-1)}(\theta) \theta^{(k)}(\mathbf{x}, \tau), \quad (32) \end{aligned}$$

$$\begin{aligned} D_j^{(k)}(\mathbf{x}, \tau) &= e_{jkl}^{(k-1)}(\theta) \varepsilon_{kl}^{(k)}(\mathbf{x}, \tau) \\ &\quad + h_{jk}^{(k-1)}(\theta) E_k^{(k)}(\mathbf{x}, \tau) + p_j^{(k-1)}(\theta) \theta^{(k)}(\mathbf{x}, \tau). \quad (33) \end{aligned}$$

It is leading to a set of linear algebraic equations for the k-th iteration step

$$\sum_{a=1}^n \left(\int_{L_s + \Gamma_{su}} \mathbf{N}(\mathbf{x}) \mathbf{C}^{(k-1)}(\mathbf{x}) \mathbf{B}^a(\mathbf{x}) d\Gamma \right.$$

$$\begin{aligned}
& -\mathbf{I}\rho(\mathbf{x})p^2 \int_{\Omega_s} \phi^a(\mathbf{x})d\Omega \Big) \hat{\mathbf{u}}^{a(k)}(p) \\
& + \sum_{a=1}^n \left(\int_{L_s+\Gamma_{su}} \mathbf{N}(\mathbf{x})\mathbf{L}^{(k-1)}(\mathbf{x})\mathbf{A}^a(\mathbf{x})d\Gamma \right) \hat{\psi}^{a(k)}(p) \\
& - \sum_{a=1}^n \left(\int_{L_s+\Gamma_{su}} \mathbf{N}(\mathbf{x})\boldsymbol{\gamma}^{(k-1)}(\mathbf{x})\phi^a(\mathbf{x})d\Gamma \right) \hat{\theta}^{a(k)}(p) \\
& = - \int_{\Gamma_{st}} \tilde{\mathbf{i}}(\mathbf{x}, p)d\Gamma - \int_{\Omega_s} \bar{\mathbf{F}}(\mathbf{x}, p)d\Omega, \quad (34)
\end{aligned}$$

$$\begin{aligned}
& \sum_{a=1}^n \left(\int_{L_s+\Gamma_{sp}} \mathbf{N}_1(\mathbf{x})\mathbf{G}^{(k-1)}(\mathbf{x})\mathbf{B}^a(\mathbf{x})d\Gamma \right) \hat{\mathbf{u}}^{a(k)}(p) \\
& - \sum_{a=1}^n \left(\int_{L_s+\Gamma_{sp}} \mathbf{N}_1(\mathbf{x})\mathbf{H}^{(k-1)}(\mathbf{x})\mathbf{A}^a(\mathbf{x})d\Gamma \right) \hat{\psi}^{a(k)}(p) \\
& + \sum_{a=1}^n \left(\int_{L_s+\Gamma_{sp}} \mathbf{N}_1(\mathbf{x})\mathbf{P}^{(k-1)}(\mathbf{x})\phi^a(\mathbf{x})d\Gamma \right) \hat{\theta}^{a(k)}(p) \\
& = - \int_{\Gamma_{sq}} \tilde{\mathbf{Q}}(\mathbf{x}, p)d\Gamma + \int_{\Omega_s} \bar{\mathbf{R}}(\mathbf{x}, p)d\Omega, \quad (35)
\end{aligned}$$

$$\begin{aligned}
& \sum_{a=1}^n \left(\int_{L_s+\Gamma_{sa}} \mathbf{N}_1(\mathbf{x})\mathbf{K}^{(k-1)}(\mathbf{x})\mathbf{A}^a(\mathbf{x})d\Gamma \right. \\
& \left. - \int_{\Omega_s} \rho(\mathbf{x})c(\mathbf{x})p\phi^a(\mathbf{x})d\Gamma \right) \hat{\theta}^{a(k)}(p) \\
& = - \int_{\Gamma_{sb}} \tilde{\mathbf{q}}(\mathbf{x}, p)d\Gamma - \int_{\Omega_s} \bar{\mathbf{W}}(\mathbf{x}, p)d\Omega. \quad (36)
\end{aligned}$$

In the 1st iteration step the material parameters are taken at a reference temperature. The iteration process is ended if the difference of the Sobolev-norms for temperatures in two successive steps is smaller than a prescribed tolerance.

4 Numerical examples

In order to test the accuracy of the present meshless method a unit square panel under a sudden heating on the top side is analyzed as the first example (Fig. 1). The following analytical solution

is available for uncoupled thermoelasticity in an isotropic material [Carslaw and Jaeger (1959)]

$$\theta(x_2, \tau) = 1 - \frac{4}{\pi} \sum_{n=0}^{\infty} \frac{(-1)^n}{2n+1} \exp \left[-\frac{(2n+1)^2 \pi^2 \kappa \tau}{4a^2} \right] \cos \left(\frac{(2n+1)\pi x_2}{2a} \right), \quad (37)$$

where a is the side-length of the panel and $\kappa = k_{22}/\rho c$ is the diffusivity coefficient.

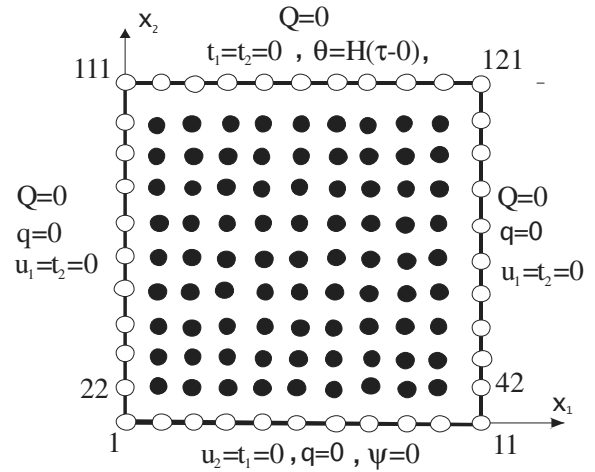


Figure 1: Uniformly heated piezoelectric square panel

Homogeneous material properties are selected to test the present computational method. The material coefficients of the panel are considered for PZT-5H (Qin and Mai, 1997)

$$\begin{aligned}
c_{11} &= 12.6 \cdot 10^{10} Nm^{-2}, & c_{12} &= 5.3 \cdot 10^{10} Nm^{-2}, \\
c_{22} &= 11.7 \cdot 10^{10} Nm^{-2}, & c_{44} &= 3.53 \cdot 10^{10} Nm^{-2}, \\
e_{15} &= 17 Cm^{-2}, & e_{21} &= -6.5 Cm^{-2}, \\
e_{22} &= 23.3 Cm^{-2}, \\
h_{11} &= 15.1 \cdot 10^{-9} C(Vm)^{-1}, \\
h_{22} &= 13 \cdot 10^{-9} C(Vm)^{-1}, \\
\rho &= 7500 kg/m^3, \\
k_{11} &= 50 W/Km, & k_{22} &= 75 W/Km, \\
\alpha_{11} &= 0.88 \cdot 10^{-5} 1/K, & \alpha_{22} &= 0.5 \cdot 10^{-5} 1/K, \\
p_1 &= 0, \\
p_2 &= -5.4831 \cdot 10^{-6} C/Km^2,
\end{aligned}$$

$$c = 420 \text{ W s kg}^{-1} \text{ K}^{-1}.$$

Also, plane strain condition is assumed. The mechanical displacement, the electrical potential and the thermal field on the finite square panel with a size $a \times a = 1 \text{ m} \times 1 \text{ m}$ are approximated by using 121 (11×11) equal-spaced nodes. The local subdomains are considered to be circular, each with a radius $r_{loc} = 0.08$. For the purpose of error analysis the Sobolev-norm is calculated. The relative error of the temperature in the considered time interval $[0, T]$ is defined as

$$r = \frac{\|\theta^{num} - \theta^{exact}\|}{\|\theta^{exact}\|}, \quad (38)$$

where $Tk_{22}/\rho ca^2 = 1.3$ and

$$\|\theta\| = \left(\int_0^T \theta^2 d\tau \right)^{1/2}.$$

Numerical results for the temperature at the bottom side and the mid-line of the panel are presented in Fig. 2. The temperature is normalized by the intensity of the thermal shock $\theta_0 = 1$. They are compared with the analytical results and an excellent agreement is observed. The relative error of the temperature, r , at both lines is less than

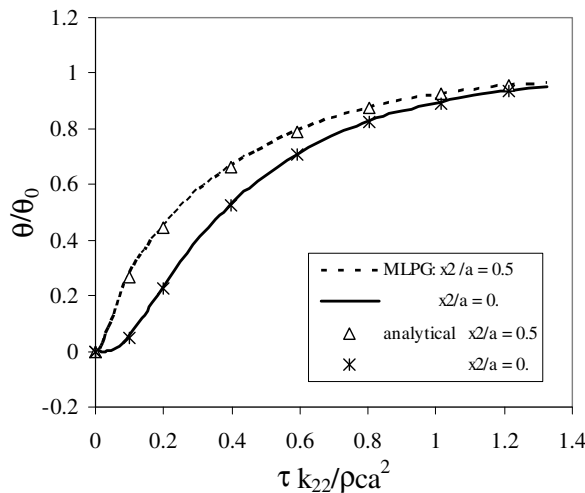


Figure 2: Temporal variation of the temperature on two different lines parallel to x_2 -axis

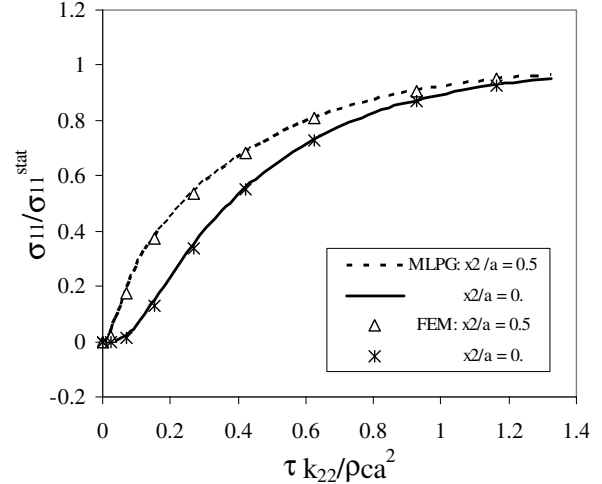


Figure 3: Temporal variation of the stress σ_{11}

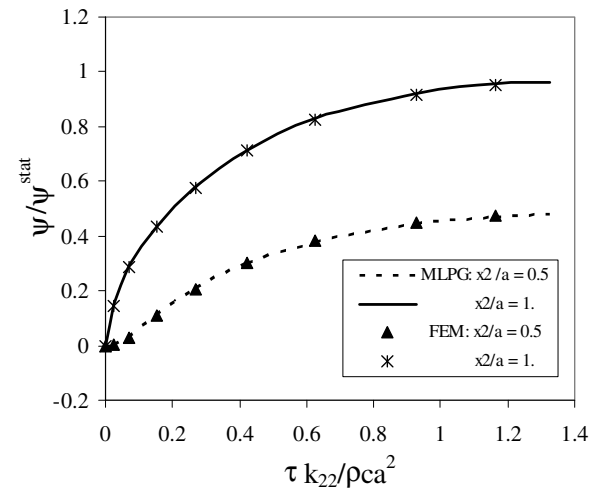


Figure 4: Temporal variation of the electrical potential at two different lines parallel to x_2 -axis

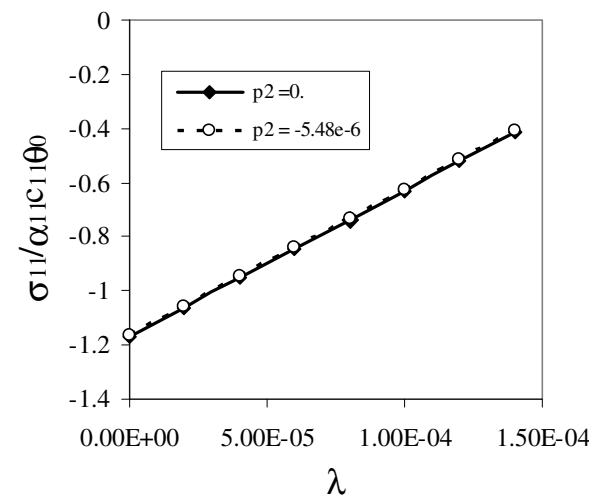


Figure 5: The influence of the electric voltage on the stress σ_{11}

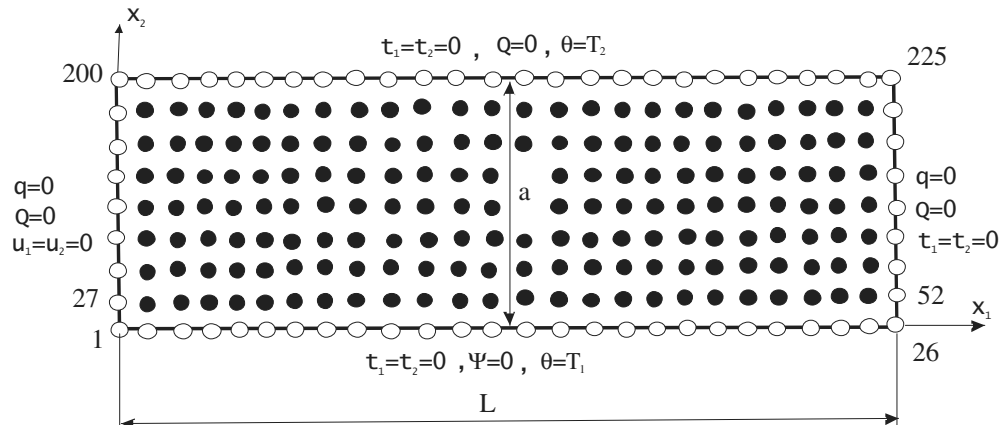


Figure 6: Cantilever piezoelectric beam under a thermal load

0.5%. For the total number of 441 nodes, the relative error $r = 0.15\%$ has been obtained. The temperature distribution is not influenced by mechanical and electrical fields.

Numerical results for the temporal variation of the direct stress σ_{11} are presented in Fig. 3, where it can be seen again that there is an excellent agreement of the present and FEM results computed at both lines considered. The FEM results have been obtained by ANSYS code with 3600 quadratic eight-noded elements and 1000 time increments. The stresses are normalized by the static value which is $\sigma_{11}^{stat} = -1.2959 \cdot 10^6 Pa$.

The temporal variation of the electrical potential ψ is shown in Fig. 4. The potential is normalized by the static quantity which is $\psi^{stat} = 1.4861 \cdot 10^4 V$ at the top side of the panel if the pyroelectric material vector $\mathbf{P}^T = (p_1, p_2)$ is vanishing. For $p_2 = -5.4831 \cdot 10^{-6} C/Km^2$ we have obtained $\psi^{stat} = 1.455 \cdot 10^4 V$. One can see that the pyroelectric parameter is only slightly decreasing the electrical potential in the considered boundary value problem.

The inverse piezoelectric effect can be utilized to control the mechanical quantities (displacements and stresses). Next, we have applied a uniform electrical displacement D_0 on the top side of the panel additionally to the thermal load. Stationary boundary conditions are considered. On Fig. 5 one can observe the influence of the electrical displacement on the stress component σ_{11} . The increasing electrical displacement on the top side of

the panel significantly reduces the normal stress. The electrical displacement is expressed through the normalized quantity $\lambda = D_0 e_{22} / h_{22} c_{11} \alpha_{11} \theta_0$. One can observe a negligible influence of the pyroelectric parameters on the stress values.

In the next numerical example a cantilever beam is analyzed. The material properties of the beam are the same like in the previous example. The geometry of the beam with a size $L \times a = 0.1 m \times 0.025 m$ is considered (Fig. 6). The lower boundary of the beam is earthed with a vanishing electrical potential. The vanishing electrical charge is prescribed on the lateral sides and on the top of the beam. The temperatures on the upper and bottom sides of the beam are prescribed as $T_2 = 1 K$ and $T_1 = 0 K$, respectively. On the lateral sides of the beam, the heat fluxes are vanishing. No mechanical load is applied to the beam.

The considered boundary value problem with respect to the thermal field is reduced to one-dimensional case. Therefore, the temperature has a linear variation along x_2 -coordinate. The variation of the deflection along the beam length is presented in Fig. 7. The deflection is computed at the neutral axis of the beam. One can observe a perfect agreement of the FEM ANSYS code and the present results obtained for negligible pyroelectric parameters. The variation of the electrical potential along the beam height is presented in Fig. 8.

Next, an edge crack in a finite piezoelectric strip is analyzed. The geometry of the strip is given

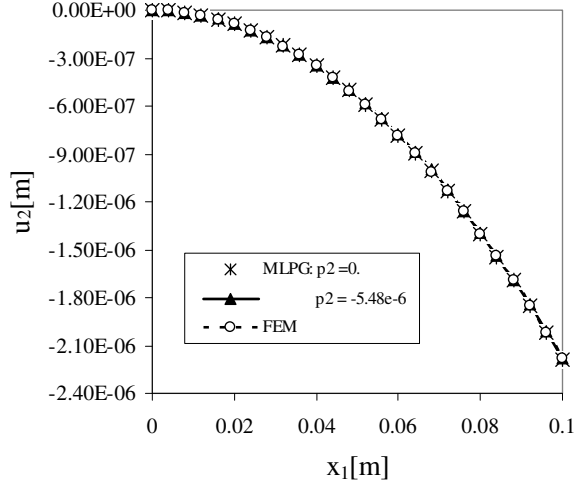


Figure 7: Variation of the deflection along the beam length

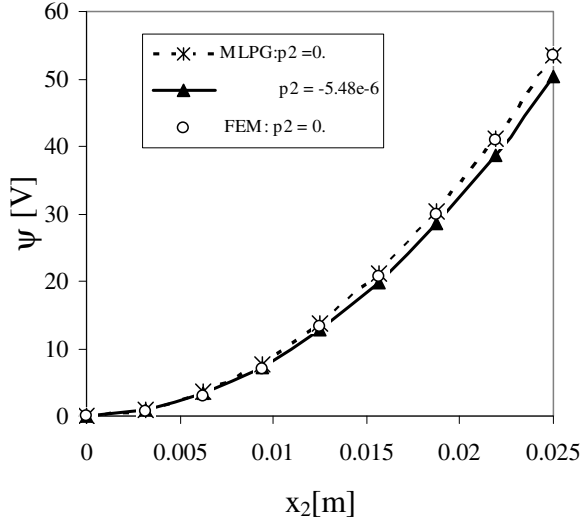


Figure 8: Variation of the electrical potential along the height of the beam at $x_1 = L/2$

in Fig. 9 with the following values: $a = 0.5$, $a/w = 0.4$ and $h/w = 1.2$. Due to the symmetry of the problem with respect to the x_1 -axis, only a half of the strip is modeled. We have used 930 nodes equidistantly distributed for the MLS approximation of the physical quantities. On the lateral sides of the strip thermal load is applied.

The crack-opening-displacement and the electrical potential computed by the present method are compared with FEM results in Fig. 10. The FEM results are obtained by the ANSYS-code with

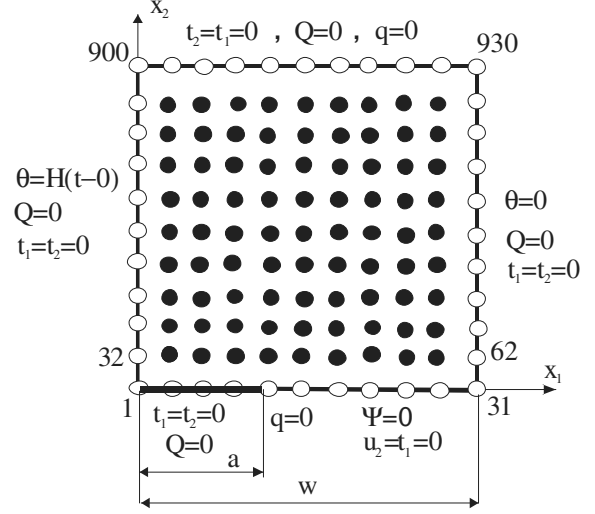


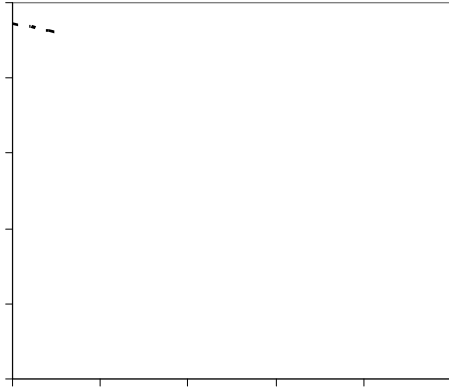
Figure 9: Edge crack in a finite strip under a thermal shock on the lateral side

8037 quadratic (8-node) elements (plane223). One can observe a good agreement of results for vanishing pyroelectric parameters. A considered finite value of the pyroelectric parameter slightly reduces the crack-opening-displacement and the absolute value of the electrical potential.

For cracks in homogeneous and linear piezoelectric solids the asymptotic behaviour of the field quantities has been given by Sosa (1991) and Pak (1992). In polar coordinates (r, ϕ) with the origin at the crack-tip, the asymptotic expressions of the electromechanical fields for $r \rightarrow 0$ can be written as

$$\begin{aligned}
 \sigma_{ij}(r, \phi) &= \frac{1}{\sqrt{2\pi r}} \sum_N K_N f_{ij}^N(\phi), \\
 D_i(r, \phi) &= \frac{1}{\sqrt{2\pi r}} \sum_N K_N g_i^N(\phi), \\
 u_i(r, \phi) &= \sqrt{\frac{2r}{\pi}} \sum_N K_N d_i^N(\phi), \\
 \psi(r, \phi) &= \sqrt{\frac{2r}{\pi}} \sum_N K_N v^N(\phi),
 \end{aligned} \tag{39}$$

where $N = I, II, III, IV, K_I, K_{II}$ and K_{III} denote the well-known mechanical stress intensity factors (SIF) and K_{IV} is the electrical displacement intensity factor (EDIF). The angular functions $f_{ij}^N(\phi)$, $g_i^N(\phi)$, $d_i^N(\phi)$ and $v^N(\phi)$ are dependent



ertia forces [Enderlein et al. (2005)]. Numerical results for the normalized stress intensity factor $f_I = K_I/\sqrt{\pi a}\alpha_{11}c_{11}\theta_0$ are presented in Fig. 11. We have also considered an induced nonhomogeneity caused by the dependence of the thermal expansion coefficient on the temperature, $\alpha_{kl} = \alpha_{kl0}(1 - m\theta)$, where $m = 0.005 K^{-1}$. One can observe that for a large instant the SIF is vanishing. The electrical displacement intensity factor (EDIF) for considered boundary value problem is vanishing.

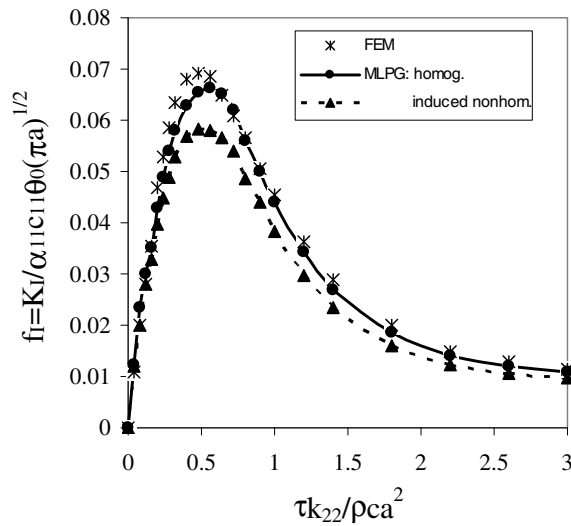


Figure 11: Time variation of the stress intensity factor for an edge crack

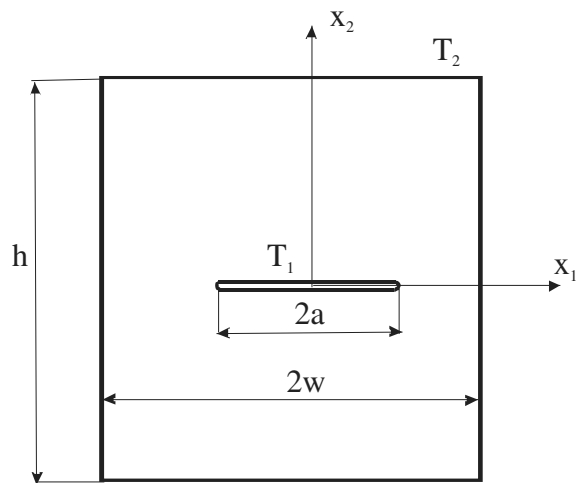


Figure 12: Central crack in a finite strip with prescribed temperatures on outer boundary and crack surfaces

Finally, a central crack in a finite piezoelectric strip is analyzed. The geometry of the strip is given in Fig. 12 with the following values: $a = 0.5$, $a/w = 0.4$ and $h/w = 1.2$. Due to the symmetry of the problem with respect to both Cartesian coordinates, only a quarter of the strip is modeled. We have used 930 nodes equidistantly distributed for the MLS approximation of the physical quantities. On the outer boundary of the strip thermal load $T_2 = \theta_0 = 1 \text{ deg}$ is applied. On both crack surfaces vanishing value of temperature is kept. The outer boundary is free of traction and electrical displacement. The material properties are the same like in the previous numerical example.

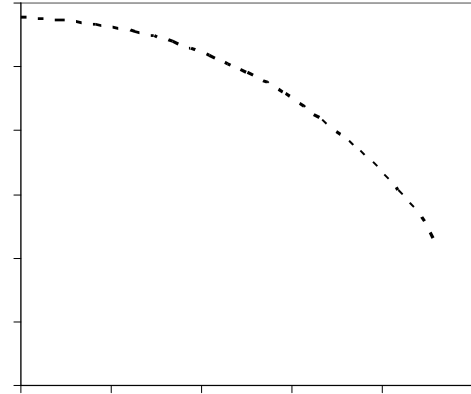
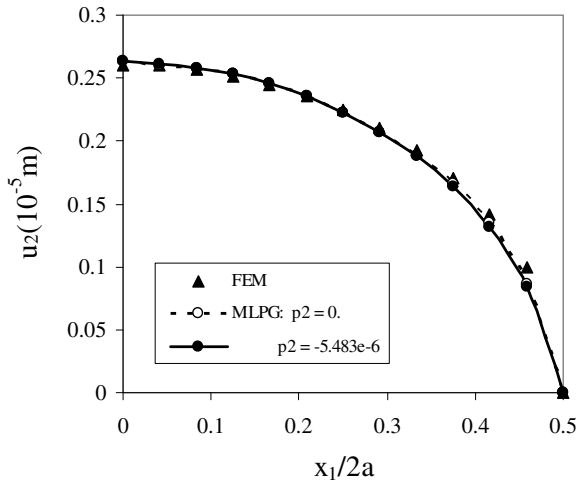
Again the crack-opening-displacement and the electrical potential computed by the present method are compared with FEM results and a good agreement of results is obtained. A negligible influence of the pyroelectric parameter at $p_2 = -5.4831 \cdot 10^{-6} C/Km^2$ on the variation of the crack-opening-displacement is observed on Fig. 13.

For the central crack under stationary boundary conditions non-zero values of thermal stresses are occurring ahead the crack tip. Therefore, a finite value of the stress intensity factor has to be obtained.

For the thermal shock boundary condition with a Heaviside time variation on the outer boundary the normalized stress intensity factors are given in Fig. 14. Again induced nonhomogeneity caused by the variation of the thermal expansion coefficient on the temperature is considered. According to Bert and Birman (1998) the effect of temperature and the electrical field on the thermal expansion coefficient can be quite significant. We have considered the same dependence like in the previous example. The time variation of the SIF is similar to that for the temperature variation in this case. The static value is reached for a large instant.

5 Conclusions

A meshless local Petrov-Galerkin method (MLPG) is proposed for the solution of boundary value problems for coupled thermo-electro-



(a)4676 340382751-2.40-4.8.3574 0 0 8.35800058.2868 569.9935 Tm010036 0 9.2

tation, since an adaptation of the nodal density is easier than a mesh adaptation. The method will be extended to 3-D problems in the next future.

Acknowledgement: The authors acknowledge the support by the Slovak Science and Technology Assistance Agency registered under number APVV-51-021205, APVT-20-035404, the Slovak Grant Agency VEGA-2/6109/27, and the German Research Foundation (DFG) under the project number ZH 15/6-1.

References

- Ashida, F.; Tauchert, T.R.; Noda, N.** (1994): Potential function method for piezothermoelastic problems of solids of crystal class 6 mm in cylindrical coordinates. *Journal of Thermal Stresses*, 17: 361-375.
- Atluri, S.N.; Zhu, T.** (1998): A New Meshless Local Petrov-Galerkin (MLPG) approach in computational mechanics, *Computational Mechanics*, 22: 117-127.
- Atluri, S.N.** (2004): *The Meshless Method (MLPG) for Domain & BIE Discretizations*, Tech Science Press.
- Atluri, S.N.; Han, Z.D.; Shen, S.** (2003): Meshless local Petrov-Galerkin (MLPG) approaches for solving the weakly-singular traction & displacement boundary integral equations. *CMES: Computer Modeling in Engineering & Sciences*, 4: 507-516.
- Atluri, S.N.; Liu, H.T.; Han, Z.D.** (2006): Meshless local Petrov-Galerkin (MLPG) mixed finite difference method for solid mechanics. *CMES: Computer Modeling in Engineering & Sciences*, 15: 1-16.
- Aouadi, M.** (2006): Generalized thermo-piezoelectric problems with temperature-dependent properties. *Int. J. Solids Structures*, 43: 6347-6358.
- Belytschko, T.; Krogauz, Y.; Organ, D.; Fleming, M.; Krysl, P.** (1996): Meshless methods; an overview and recent developments. *Comp. Meth. Appl. Mech. Engineering*, 139: 3-47.
- Bert, C.W.; Birman, V.** (1999): Stress dependency of the thermoelastic and piezoelectric coefficients. *AIAA Journal*, 37: 135-137.
- Carslaw, H.S.; Jaeger, J.C.** (1959): *Conduction of Heat in Solids*, Clarendon, Oxford.
- Ding, H.; Liang, J.** (1999): The fundamental solutions for transversely isotropic piezoelectricity and boundary element method. *Computers & Structures*, 71: 447-455.
- Dunn, M.L.** (1993): Micromechanics of coupled electroelastic composites: Effective thermal expansion and pyroelectric coefficients. *Journal of Applied Physics*, 73: 5131-5140.
- Enderlein, M.; Ricoeur, A.; Kuna, M.** (2005): Finite element techniques for dynamic crack analysis in piezoelectrics. *International Journal of Fracture*, 134: 191-208.
- Garcia-Sanchez, F.; Saez, A.; Dominguez, J.** (2005): Anisotropic and piezoelectric materials fracture analysis by BEM. *Computers & Structures*, 83: 804-820.
- Garcia-Sanchez, F.; Zhang, Ch.; Sladek, J.; Sladek, V.** (2007): 2-D transient dynamic crack analysis in piezoelectric solids by BEM. *Computational Materials Science*, 39: 179-186.
- Gornandt, A.; Gabbert, U.** (2002): Finite element analysis of thermopiezoelectric smart structures. *Acta Mechanica*, 154: 129-140.
- Govorukha, V.; Kamlah, M.** (2004): Asymptotic fields in the finite element analysis of electrically permeable interfacial cracks in piezoelectric bimaterials. *Archives Applied Mechanics*, 74: 92-101.
- Gruebner, O.; Kamlah, M.; Munz, D.** (2003): Finite element analysis of cracks in piezoelectric materials taking into account the permittivity of the crack medium. *Eng. Fracture Mechanics*, 70: 1399-1413.
- Gross, D.; Rangelov, T.; Dineva, P.** (2005): 2D wave scattering by a crack in a piezoelectric plane using traction BIEM. *SID: Structural Integrity & Durability*, 1: 35-47.
- Han, F.; Pan, E.; Roy, A.K.; Yue, Z.Q.** (2006): Responses of piezoelectric, transversely isotropic, functionally graded and multilayered half spaces to uniform circular surface loading.

CMES: Computer Modeling in Engineering & Sciences, 14: 15-30.

Kuna, M. (2006): FEM-techniques for thermo-electro-mechanical crack analyses in smart structures. In: *IUTAM Symposium on Mechanics and Reliability of Actuating Materials* (Yang Wei, ed.), Springer, Beijing, 131-143.

Kuna, M. (2006): Finite element analyses of cracks in piezoelectric structures – a survey. *Archives of Applied Mechanics*, 76: 725-745.

Lee, J.S. (1995): Boundary element method for

plane piezoelectricity. *Computational Mechanics*, 37: 381-393.

Sladek, J.; Sladek, V.; Atluri, S.N. (2004): Meshless local Petrov-Galerkin method in anisotropic elasticity. *CMES: Computer Modeling in Engineering & Sciences*, 6: 477-489.

Sladek, J.; Sladek, V.; Zhang, Ch.; Garcia-Sanchez, F.; Wunsche, M. (2006): Meshless local Petrov-Galerkin method for plane piezoelectricity. *CMC: Computers, Materials & Continua*, 4: 109-118.

Sladek, J.; Sladek, V.; Zhang, Ch.; Solec, P.; Starek, L. (2007): Fracture analyses in continuously nonhomogeneous piezoelectric solids by the MLPG. *CMES: Computer Modeling in Engineering & Sciences*, 19: 247-262.

Sosa, H. (1991): Plane problems in piezoelectric media with defects. *Int. J. Solids Structures*, 28: 491-505.

Stehfest, H. (1970): Algorithm 368: numerical inversion of Laplace transform. *Comm. Assoc. Comput. Mach.*, 13: 47-49.

Tsamasphyros, G.; Song, Z.F. (2005): Analysis of a crack in a finite thermopiezoelectric plate under heat flux. *International Journal of Fracture*, 136: 143-166.

Tzou, H.S.; Ye, R. (1994): Piezothermoelasticity and precision control of piezoelectric systems: Theory and finite element analysis. *Journal of Vibration and Acoustics*, 116: 489-495.

Ueda, S. (2003): Crack in functionally graded piezoelectric strip bonded to elastic surface layers under electromechanical loading. *Theoretical Applied Fracture Mechanics*, 40: 225-236.

Yu, S.W.; Qin, Q.H. (1996a): Damage analysis of thermopiezoelectric properties: Part I – Crack tip singularities. *Theoretical Applied Fracture Mechanics*, 25: 263-277.

Yu, S.W.; Qin, Q.H. (1996b): Damage analysis of thermopiezoelectric properties: Part II – Effective crack model. *Theoretical Applied Fracture Mechanics*, 25: 279-288.

Zhu, T.; Zhang, J.D.; Atluri, S.N. (1998): A local boundary integral equation (LBIE) method in computational mechanics, and a meshless dis-

cretization approaches. *Computational Mechanics*, 21: 223-235.

Zhu, X.; Wang, Z.; Meng, A. (1995): A functionally gradient piezoelectric actuator prepared by metallurgical process in PMN-PZ-PT system. *J. Mater. Sci Lett.*, 14: 516-518.

Zhu, X.; Zhu, J.; Zhou, S.; Li, Q.; Liu, Z. (1999): Microstructures of the monomorph piezoelectric ceramic actuators with functionally gradient. *Sensors Actuators A*, 74: 198-202.

